Chinese Journal of Chemical Engineering 87 (2025) 313–322

Contents lists available at ScienceDirect

Chinese Journal of Chemical Engineering

journal homepage: www.elsevier.com/locate/CJChE

Full Length Article

Mechanistic insights into water desalination through two-dimensional MXene-graphene oxide membranes: A molecular simulation study

Jie Liu *, Xiaoyan Tan , Yibo Xu , Zijuan Li , Yanan Xue , Faquan Yu *

Hubei Key Laboratory for Novel Reactor and Green Chemistry Technology, WIT-Qianjiang Research Institute of Green Chemical Industry, School of Chemical Engineering and Pharmacy, Wuhan Institute of Technology, Wuhan 430205, China

ARTICLE INFO

Article history:
Received 17 December 2024
Received in revised form
10 April 2025
Accepted 5 May 2025
Available online 18 July 2025

Keywords:
Two-dimensional membrane
MXene
Graphene oxide
Desalination
Molecular dynamics simulation

ABSTRACT

The emerging two-dimensional (2D) membranes offer a promising way to improve the water desalination performance of traditional membranes. MXene/graphene oxide (GO) composite membrane are known for their high separation performance and structural stability. In this study, molecular simulations are performed to investigate the desalination performance of the 2D MXene/GO membrane. The results reveal that the surface of the MXene nanosheet could induce the formation of ordered water structures, thereby accelerating the water transport in the 2D membrane. The higher rejection rate would be found in MXene/GO membrane with a larger GO oxidation degree owing to the steric-hindrance effect induced by the functional groups on the GO surface. Overall, the MXene/GO(20) membrane with the interlayer spacing of 0.9 nm shows the highest water permeability (37.22×10^{-7} L·m^{-1}·h^{-1}·bar^{-1}, 1 bar = 0.1 MPa) and a salt rejection of 100%. The results could provide theoretical insights for developing 2D membranes for water desalination.

1. Introduction

The scarcity of freshwater resources is a pivotal challenge in the 21st century [1]. Seawater can alleviate freshwater shortages, as it accounts for 97% of the water resources in the world [2]. Water desalination has become the most feasible solution to increase freshwater resources [3]. Due to the advantages of low energy consumption, ease of operation, and eco-friendliness, membrane separation has been broadly applied in water desalination [4,5]. However, conventional membrane materials generally face the "trade-off" effect between high permeability and selectivity. Due to the atomic thickness, the two-dimensional (2D) layered membranes could greatly reduce the transport resistance of molecules. With the help of Poiseuille's law, the purpose of maximizing permeability is achieved [6]. At present, a large number of two-dimensional (2D) materials have been studied and developed into separation membranes and applied to the field of water desalination [7,8], such as graphene oxide (GO) [9,10], hexagonal boron nitride (h-BN) [11,12], molybdenum disulfide (MoS_2) [13–16], graphitic carbon nitride (g-C_3N_4) [17,18] and MXene [19,20].

MXene, a novel 2D metal carbide/carbonitride flake, has emerged as a promising material for water desalination due to its hydrophilicity, high specific surface area, ease of functionalization, and abundance of activated metal hydroxide sites [21–23]. In 2015, Ren *et al.* [24] firstly fabricated the $Ti_3C_2T_x$ membranes using a vacuum-assisted filtration (VAF) method, and the water flux was up to 37.4 L·m^{-1}·h^{-1}·bar^{-1} (1 bar = 0.1 MPa). Ding *et al.* [25] reported a 2D layered MXene membrane with a favorable rejection rate (more than 90%) and exceptional water permeance (over 1000 L·m^{-2}·h^{-1}·bar^{-1}) for molecules larger than 2.5 nm in size. Subsequently, this group reported a series of MXene membranes prepared by Al^{3+} ions intercalation to reduce the swelling of 2D membranes in water. They achieved an excellent non-swelling stability of 2D membrane in aqueous solutions over 400 h. The water fluxes were about 1.1–8.5 L·m^{-2}·h^{-1}, along with a high rejection of NaCl (~89.5%–99.6%) [26]. Jin *et al.* [27] utilized electrostatic interactions and size sieving to construct surface charged MXene membranes, which exhibited excellent water permeability and high salt rejection during nanofiltration or forward osmosis processes. To improve the nanofiltration and anticontamination properties of the membranes, Luo *et al.* [28] reported a variety of

* Corresponding authors.
E-mail addresses: ljie@wit.edu.cn (J. Liu), fyu@wit.edu.cn (F. Yu).

https://doi.org/10.1016/j.cjche.2025.05.033

amino acid-bonded $Ti_3C_2T_x$ MXene membranes and found enhanced water permeance (7.17–13.11 $L \cdot m^{-2} \cdot h^{-1} \cdot bar^{-1}$). Besides, the Gly-bonded membrane exhibited enhanced anti-fouling characteristics and an 80.59% flow recovery rate in relation to bovine serum albumin (BSA). Pandey *et al.* [29] reported that the 2D MXene ($Ti_3C_2T_x$) modified by Ag nanoparticles exhibited a water permeance of ~420 $L \cdot m^{-2} \cdot h^{-1} \cdot bar^{-1}$ and enhanced bactericidal properties. Although metal-intercalated MXene has been reported to enhance salt rejection, the pure MXene membranes still face some limitations, like stability [26].

Developing an MXene/graphene oxide (GO) membrane is a new choice for enhancing separation performance [30–32]. Ma *et al.* [30] fabricated the 2D MXene/GO membrane and achieved high water permeability (136.68 $L \cdot m^{-2} \cdot h^{-1} \cdot bar^{-1}$) with excellent rejection (>99.99%) for various dyes. Chang *et al.* [33] reported that the enhancement of water permeability was mainly caused by the insertion of small MXene-NH_2 into the gap of GO layers, which could increase the vertical distance between GO layers and shorten the water transport pathways. Generally, MXene/GO membranes exhibit lower water permeability than pristine MXene membranes [33–35]. Many reported works, they mainly attributed this trend to the expanded interlayer spacing, which could increase the transport path [30,33,34,36]. To the best of our knowledge, most studies focused on the separation performances of the MXene/GO membrane. Still, the mechanism of water transport through the MXene/GO membrane, which is crucial for new membrane development, has seldom been reported.

Molecular dynamics (MD) simulation is an effective way to unravel the transport mechanisms of molecules across membranes [16,37,38]. Fan's group [39–41] performed a sequence of simulation works to study the water desalination through the MXene membrane and discussed the effects of many factors, including terminal groups and arrangement of MXene. They pointed out that the surface charge features and the hydrogen bond interactions dominated the interactions of the MXene membrane with water. A comparison between 2D membranes was studied by Ang *et al.* [42], the results showed that the shape of the slits, the hydrophobicity, and the inherent interaction parameters of the membranes played the dominant roles in the desalination determination. Meidani *et al.* [43] performed MD simulations to investigate the water desalination performance through nanoporous single-layer MXene membranes. They found that the water flux can be well tuned by the pore chemistry. It follows from the above that MD simulation can be used to directly reveal the desalination mechanism of 2D membrane and predict the desalination performance.

This work systematically sudies the desalination performance of 2D MXene/GO membranes using molecular dynamics simulation. Different interlayer spacings and the oxidation degrees of GO nanosheets in the membranes are considered, and the pure GO as well as pure MXene membranes are also studied as benchmarks. Section 2 describes the models and simulation methods. The main factors governing water transport in 2D membranes are discussed in Section 3. The water permeability and salt rejection are also predicted. Finally, the concluding remarks are summarized in Section 4.

2. Models and Methods

The MXene and GO nanosheets were constructed with the size of 5.5 nm × 5 nm in the *x*-*y* plane, as illustrated in Fig. 1a. The molecular formula of the MXene nanosheet was $Ti_3C_2O_2$. GO nanosheet with different oxidation degrees were constructed by varying the number of hydroxyl and epoxy groups on the graphene sheet [44]. The oxidation degree here was defined as $d_O = n_O/n_C \times 100\%$, where n_O is the number of oxygen atoms, and n_C is the number of carbon atoms [45]. Based on reported experimental works, the oxidation degrees of GO were typically between 10% and 44% [46–49]. Therefore, three oxidation degrees, including 10% (labeled as GO(10)), 20% (labeled as GO(20)), and 40% (labeled as GO(40)), were considered in this work. The geometric optimization was performed for all the GO nanosheets. Therefore, the GO nanosheets shown in Fig. 1(a) are not flat. Interlayer spacing (labeled as *d* in figures) is also one of the key factors determining the flux and selectivity of 2D membrane materials. The interlayer spacings of experimentally synthesized MXene/GO membranes ranged from 0.77 nm to 1.81 nm [36,50–52]. Therefore, four interlayer spacings were set, including 0.6, 0.9, 1.2, and 1.5 nm. It

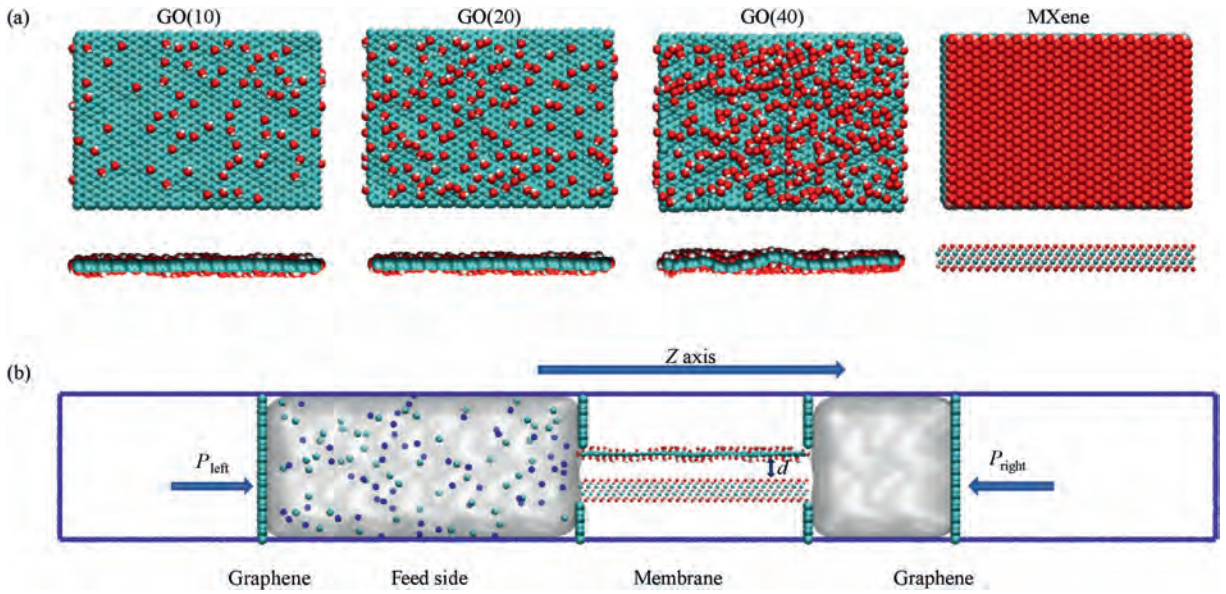

Fig. 1. (a) The top and side views of GO and the MXene nanosheets. (b) The model of water desalination system. Na^+ and Cl^- ions are presented by blue and cyan spheres, respectively.

was worth mentioning that the interlayer spacing was defined as the distance between the carbon layer in GO and the surface of MXene. The nanosheets were kept fixed during the simulation to maintain the specific interlayer spacing.

The model for predicting desalination performance is shown in Fig. 1(b). Two nanosheets are stacked on top of each other to create a horizontal nanochannel. Then, each membrane was placed in the middle of the box and sandwiched by the feed and permeate chambers. The dimensions of the simulation box were about 5.5 nm × 5 nm × 40 nm. To eliminate the periodic effect in the *z*-axis, two vacuum boxes were added at each end of the box along the *z*-axis. Although the system remains three-dimensional, this setup effectively mimics a situation similar to that of a pseudo-2D system by eliminating the movement of molecules through the boundary in the *z*-direction. The impermeable walls were placed at the edges of the membrane to restrict the movement of the molecules to the regions outside the membrane. During the simulation, the position of membrane was fixed in three dimensions. In addition, as pistons, two graphene plates were placed on the left and right sides of the box, respectively. A high pressure difference (60 MPa) was applied to the system by applying pressures of 60.1 MPa and 0.1 MPa to the graphene plates on the left and right, respectively. In the nanosecond simulations, such a high pressure difference ensured a reduction in thermal noise and an increase in signal-to-noise ratio [53]. The NaCl concentration of 0.35 mol·L^{-1} was considered in the feed side to mimic seawater [54,55]. In the system, the membrane and ions are described by OPLS-AA force field [56], and water molecules are described by the TIP3P model [57].

The water desalination process was simulated by non-equilibrium dynamics simulation (NEMD) [58–60]. The GROMACS v2018 software package [61] was used. Each system first underwent an energy minimization process, then followed by NEMD. In energy minimization, the maximum step size was 0.05 nm, and the force tolerance was 1000 kJ·mol^{-1}·m^{-1}. According to the Maxwell-Boltzmann distribution, the primary velocities of the atoms were assigned at 300 K. In the MD simulation, the temperature was maintained at 300 K. The coupling time constant was 0.1 ps, and the v-rescale thermostat [62] was used. The Lennard-Jones (LJ) interactions were calculated with a cutoff of 1.40 nm. The Particle Mesh Ewald (PME) method [63,64] was employed for the electrostatic interactions. A time step of 2 fs was used, and the trajectory was saved every 10 ps. Each snapshot was generated and rendered by Visual Molecular Dynamics (VMD) software [65]. To ensure sufficient sampling, each system was simulated for at least 20 ns, and the longer simulation time was performed for specific systems based on the linear growth of water flux. The results from the last 10 ns of the NEMD after the system reached equilibrium were collected for data analysis. To ensure the accuracy and reproducibility of the simulations, each system was simulated individually at least three times, and all the results were averaged over the three independent runs.

3. Results and Discussion

Firstly, the water permeabilities of MXene/GO, pure GO, and pure MXene membranesare characterized. The influence of interlayer spacing on permeability is discussed in detail. Additionally, the roles of MXene and GO nanosheets in water transport are analyzed, and salt rejection performance is predicted.

3.1. Water permeability

The net water flow (N_W) through 2D MXene/GO membranes is simulated and shown in Fig. 2. Initially, N_W is negligible due to the time required for water molecules to permeate the membrane. After this lag phase, N_W increases linearly with simulation time. Notably, for membranes with narrow interlayer spacing (*e.g.*, 0.6 nm), N_W remains negligible even in 20 ns simulations, necessitating extended simulations (Figs. S1–S4).

The water permeability can be estimated from

$$P_s = \frac{(N_W/N_A)\cdot N_W \cdot l}{A\cdot \Delta t\cdot \Delta p}$$

where N_W and N_A is the molecular weight of water and the Avogadro constant (6.022×10^{23}), respectively. l is the membrane thickness, A is the cross section area of the membrane, Δt is the time duration when N_W linearly increases, Δp is the pressure difference. The water permeabilities through membranes with different compositions and interlayer spacings are shown in Fig. 3 and listed in Table S1. The water permeabilities of the MXene/GO membrane calculated in this work are comparable to other experimentally reported results [35,52,66]. It can be observed from Fig. 3 that, for the same membrane composition, the water permeability accordingly increases with the increasing interlayer spacing. A similar trend has also been reported in previous works [31,34,35,52]. It is clear that a wider interlayer spacing would obviously increase the space in the 2D membrane for water molecules to transfer, thus enhancing the water permeability. Additionally, Fig. 3 shows that, under the same oxidation degree of GO and interlayer spacing, the water permeabilities through the membranes follow the sequence of pure MXene > MXene/GO > pure GO, which is consistent with experimental results [66]. Moreover, with the same interlayer spacing, the water permeabilities decrease with the increasing oxidation degree of the GO nanosheet. These phenomena will be discussed in detail below.

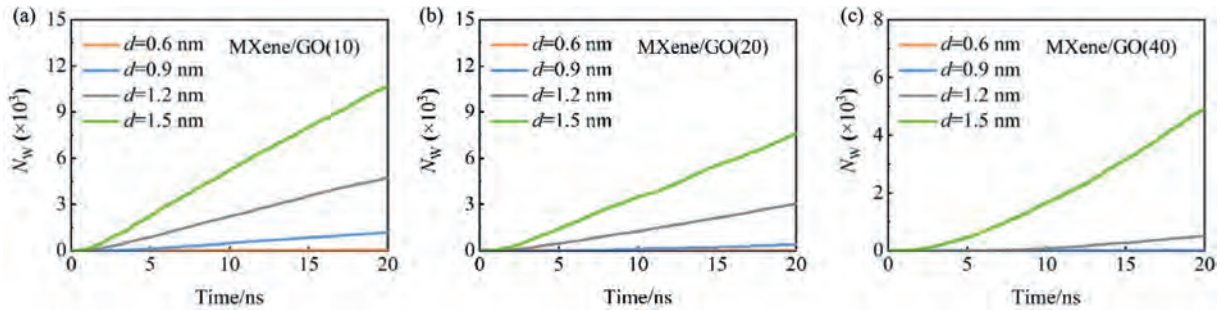

Fig. 2. Net water flows (N_W) *versus* time t through (a) the MXene/GO(10), (b) the MXene/GO(20), and (c) the MXene/GO(40) membranes.

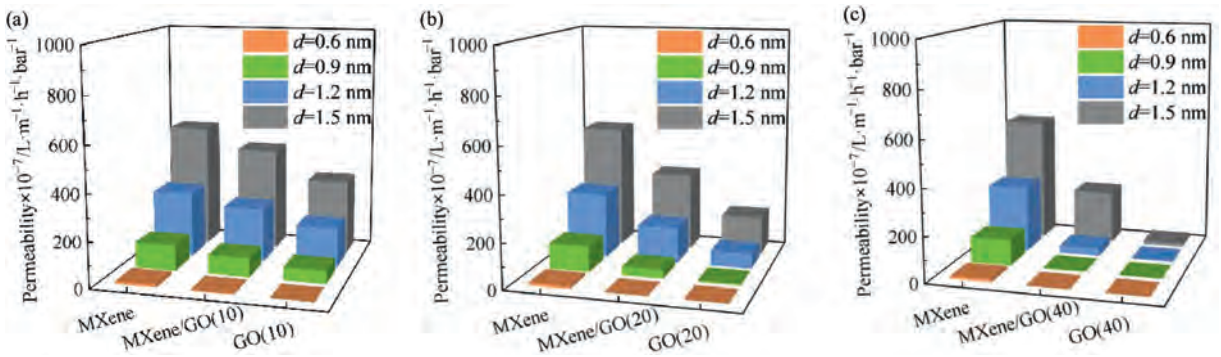

Fig. 3. Water permeabilities through (a) the MXene/GO(10), (b) the MXene/GO(20), and (c) the MXene/GO(40) membranes. Water permeabilities through pure MXene and pure GO membranes are plotted for comparison.

3.2. Effects of MXene nanosheet on water transport

As mentioned above, the water permeability distinctly increases with the insertion of the MXene nanosheet in the 2D membrane. To illustrate this, the diffusion of water molecules in membranes along the *z*-axis is analyzed using the diffusion coefficient (D)

$$D = \lim_{t\to\infty} \frac{1}{6t}\left(\frac{1}{N}\sum_{i=1}^{N}\langle|z_i(t) - z_i(0)|^2\rangle\right)$$

where t is the time, N is the number of molecules, $z_i(t)$ is the position of molecule i, and $< \cdots >$ is the ensemble average. Taking membranes with the GO(10) nanosheets as examples, Fig. 4 shows the diffusion coefficient of water inside the membrane along the z-axis. The values are in the same order of magnitude as the reported works [67–70]. The incorporation of MXene significantly enhances water diffusion, as evidenced by the diffusion coefficient (Fig. 4) and the mean-squared displacement (MSD) (Fig. S5). Water diffusion follows the sequence pure MXene > MXene/GO > pure GO, consistent with observed permeability trends for all interlayer spacing. The MXene nanosheets improve water transport by lowering interfacial resistance and promoting ordered water structures (Figs. 5–7). It can be inferred that the diffusion of water molecules in the membrane could be accelerated by the MXene nanosheets. Notably, even with the interlayer spacing up to 1.5 nm, among the three 2D membranes, the MSD_z of water in pure MXene

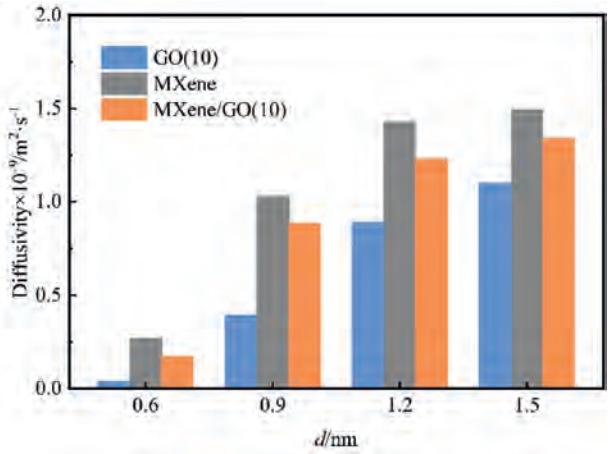

Fig. 4. The diffusivity coefficient of water inside the GO(10), pure MXene, and the MXene/GO(10) membranes along the *z*-axis.

is still the largest one, indicating that the interfacial effect of nanosheet plays a significant role in determining water permeability.

To illustrate the distribution of intercalated water molecules, the density profiles of water molecules along the normal direction of the nanosheet (*y*-axis) in the membrane are analyzed and shown in Fig. 5. With the interlayer spacing increasing from 0.6 nm to 1.5 nm, the distribution of water molecules in the channels becomes wider (Fig. 5), and the density peaks near the nanosheets are distinctly sharper than others. This implies that the interfacial effect of nanosheets plays a pivotal role in the structure and transport of water in confined channels, and also manifests that the water permeability can be well-tuned by different nanosheets. Similar results have also been reported in previous studies [71].

In the membranes with an interlayer spacing of 0.6 nm, a single-layer density peak can be observed between nanosheets (Fig. 5). This is in good agreement with the experimental result that only one layer of water molecules can be accommodated in such a narrow channel [72]. This single-layer profile reflects the interfacial effects of nanosheets on water structure in membranes with a 0.6 nm interlayer spacing. Therefore, we further examine the orientation distribution of water molecules in these membranes, including pure MXene, MXene/GO, and pure GO membranes (shown in Fig. 6 and S6). The orientation ($\cos\theta$) is defined as the cosine value of the angle between the dipole moment of water and the normal axis of the nanosheet. In the pure GO(10) membrane, the water molecules are randomly oriented since the values of $\cos\theta$ range from -1 to $+1$. Intriguingly, with the addition of MXene, the orientation distribution of water molecules in the membrane becomes more concentrated. Especially in the pure MXene membrane, the orientations of water molecules are highly ordered with the $\cos\theta$ value of 0.99, which indicates that the angle between the dipole moment of water molecules and the normal axis of the nanosheet is zero.

From the 2D density profiles of water molecules in membranes (Fig. 7), it can also be found that, in the pure GO(10) membrane, the water molecules prefer to cluster around the hydroxyl and epoxy groups on the GO nanosheet. In the pure MXene membrane, the water structures are highly ordered and form a square ice structure. As expected, the distribution of water molecules in the MXene/GO(10) membrane becomes more ordered than that in the pure GO(10) membrane. As reported in previous works, an ordered structure of water molecules in nanochannels would result in a faster flow [71,73]. Therefore, based on the results of orientation distributions and 2D density profiles of water in the membranes, it can be deduced that, compared with the pure GO membrane, the higher water permeability through MXene/GO membrane is

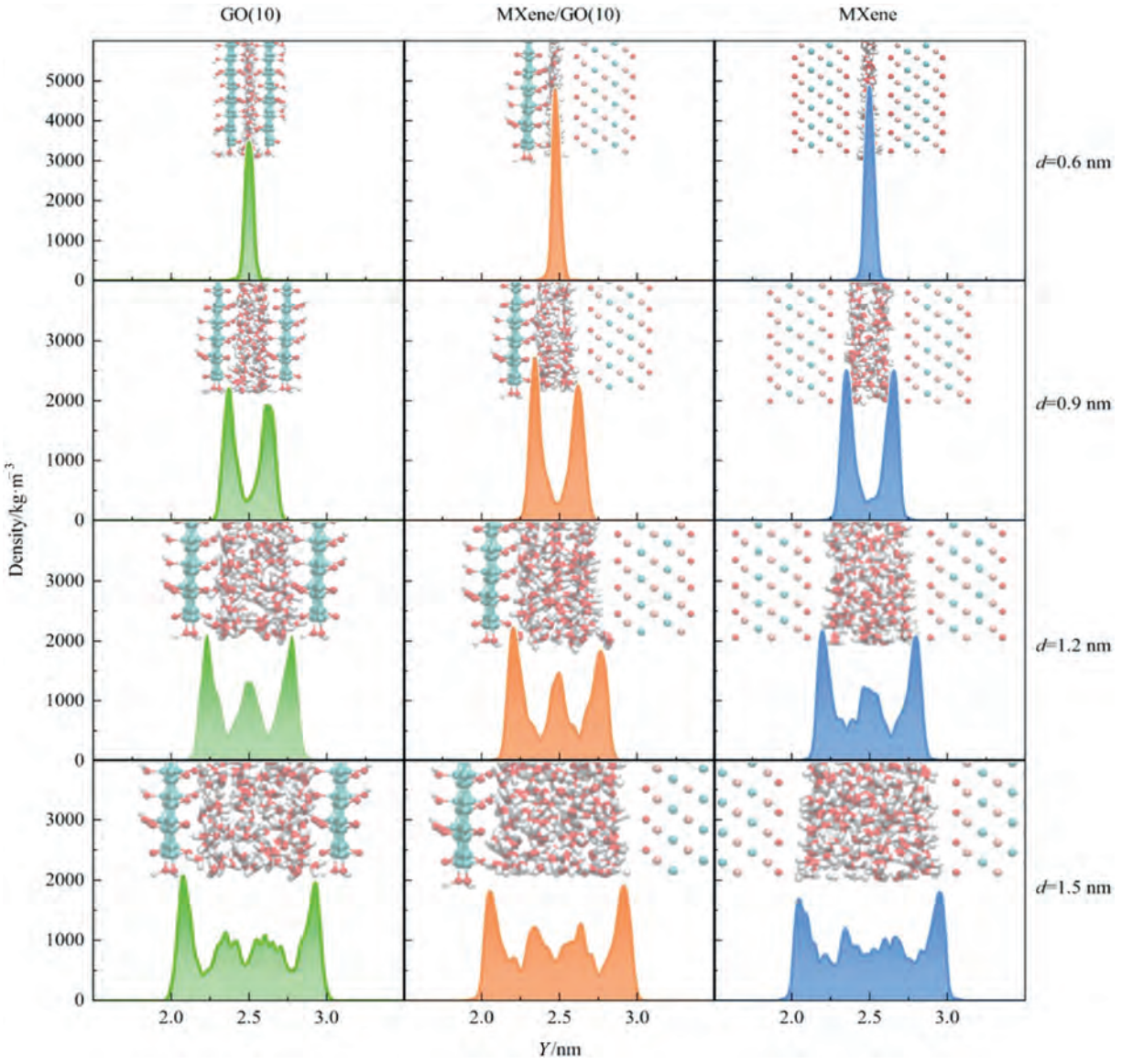

Fig. 5. Density profiles of water in the GO(10), pure MXene, and the MXene/GO(10) membranes along the *y*-axis (*i.e.*, the normal direction of the nanosheet). The inner configurations are the snapshots of water molecules in the membranes.

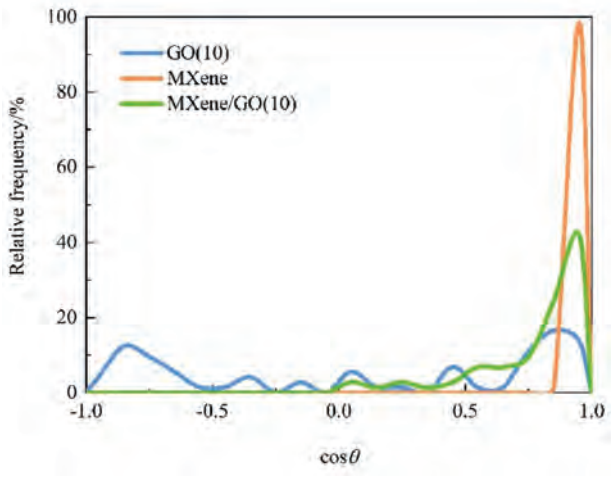

Fig. 6. Orientation distributions of water molecules in the GO(10), pure MXene, and the MXene/GO(10) membranes. The interlayer spacing is 0.6 nm.

mainly attributed to the ordered water structures in the 2D membrane, which is induced by the MXene surface.

Analyzing the evolution of the potential of mean force (PMF) along the membrane channel is an efficient way to describe the energy barrier for water permeation. The PMF is calculated from

$$F(z) = -RT\ln[\rho(z)/\rho_0]$$

where R is the gas constant, T is the temperature, $\rho(z)$ is the density profile of water in the membrane along the z-axis, ρ_0 is the bulk density of water. Again, taking the interlayer spacing of 0.6 nm and oxidation degree of 10% as examples, the PMFs of water through the membranes are evaluated and plotted in Fig. 8. Pure GO(10) and MXene membrane are also considered as benchmarks. As shown in Fig. 8, for pure GO(10) and MXene/GO(10) membranes, the maximum value of PMF appears in the membrane. However, for MXene membranes, the maximum value of PMF is observed at the entrance. It can be inferred that the interaction between water and GO(10) surface plays the dominant role in the water transport resistance, and the interaction between water and MXene surface

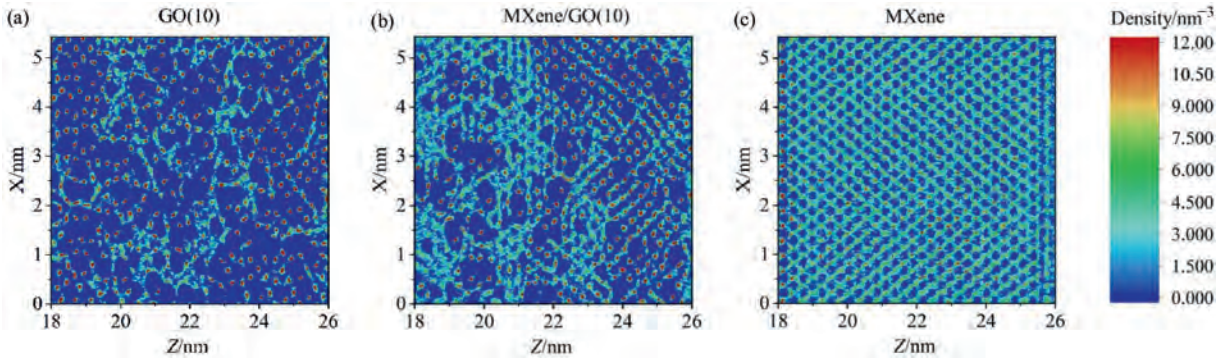

Fig. 7. 2D density profiles of water molecules in the *x-z* plane between the nanosheets in the GO(10), pure MXene, and the MXene/GO(10) membranes. The interlayer spacing is 0.6 nm.

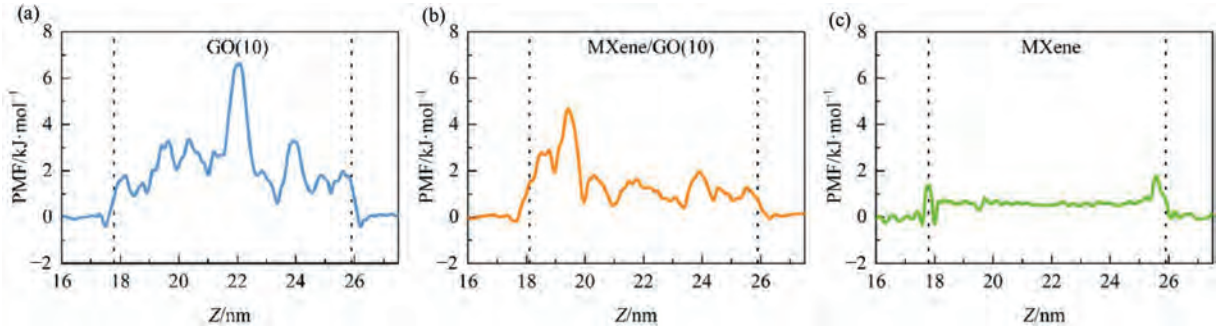

Fig. 8. PMF of water through the GO(10), the MXene/GO(10), and pure MXene membranes along the *z*-axis. The dotted lines indicate the position of membrane, the interlayer spacings of the membranes are 0.6 nm.

does not crease much resistance. From the minimal to the maximal value in the PMF curve, the overall free energy barriers through pure GO(10), MXene/GO(10), and pure MXene membranes are 7.39, 4.69, and 2.20 kJ·mol^{-1}, respectively. This again evidences that adding the MXene in the 2D membrane would drop the transport resistance of water molecules in the membrane and thus efficiently facilitate the water flux.

3.3. *Effects of GO oxidation degree on water transport*

As shown in Fig. 3, the water permeability decreases with increasing oxidation degree of GO nanosheets. To illustrate this, the interaction energies between water and membrane are examined and shown in Fig. 9a. To elucidate the effect of oxidation degree on the water molecule transfer in a more rational manner, the system with a layer spacing of 0.9 nm is taken as a typical case. Apparently, the total interaction energies between water and membranes increase with the increasing oxidation degree of the GO nanosheet. Based on this, it can be inferred that a higher oxidation degree of the GO nanosheet would enhance the transport resistance of water in the MXene/GO membrane, therefore slowing down the water permeability. Similar results have also been reported in previous works [73,74]. Moreover, electrostatic interactions play the dominant roles for all three membranes

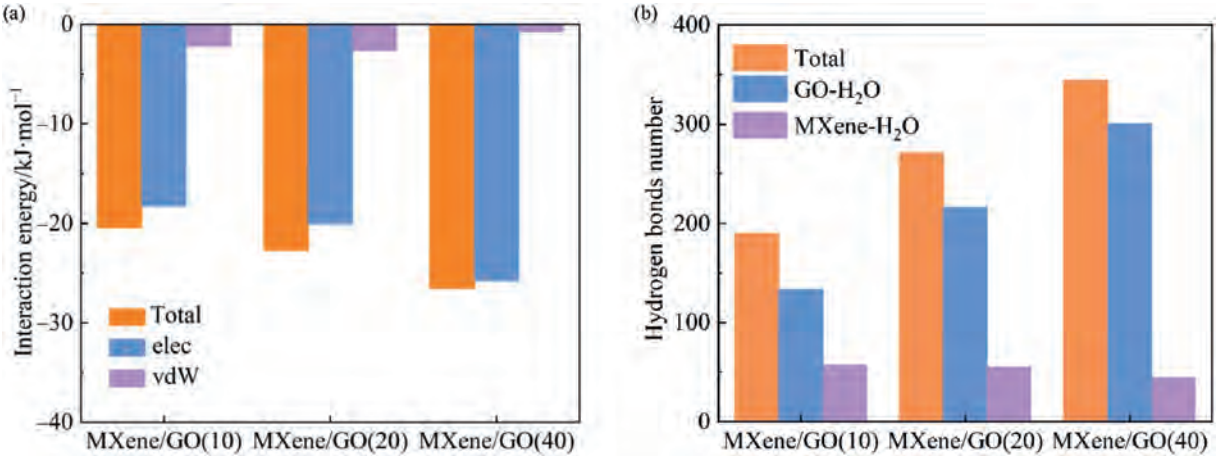

Fig. 9. The (a) interaction energy and (b) number of hydrogen bonds between water molecules and MXene/GO membranes with an interface spacing of 0.9 nm.

shown in Fig. 9(a). The total number of hydrogen bonds between water and membrane, as well as the one between water and each nanosheet, are further analyzed and depicted in Fig. 9(b). It is straightforward to find that the number of hydrogen bonds increases with the increasing oxidation degree of GO nanosheet. Besides, the number of hydrogen bonds between water and MXene nanosheet changes marginally, while the one between water and GO nanosheet increases distinctly with the increasing oxidation degree. This observation is again rooted at why the higher oxidation degree of GO in the MXene/GO membrane could enhance the electrostatic interactions between water and membranes and decrease the water permeability.

The dynamics of hydrogen bonds in the membrane is further examined by the autocorrelation function (ACF)

$$c(t) = \frac{\langle h_{ij}(t_0) h_{ij}(t_0 + t) \rangle}{\langle h_{ij}(t_0) h_{ij}(t_0) \rangle}$$

where $h_{ij}(t)$ represents a hydrogen bond between a water molecule and oxygen functional group at time t_0.When a hydrogen bond is not formed, the $h_{ij}(t)$ equals to zero. The $< \cdots >$ is the ensemble average over all pairs of hydrogen-bonded water molecules. The ACF is calculated by an in-house code. For the ACF of hydrogen bonds in membranes, a new box is constructed with the membrane and the water molecules in the layers only. For the calculation of ACF in bulk, a box with bulk water is constructed. A 20 ps simulation is further performed. The ACF ($c(t)$) can be used to quantitatively assess the rate of hydrogen bonds relaxation and examine the probability of a water molecules pair that maintains hydrogen-bonded at time $t = t_0$ and $t + t_0$. Taking MXene/GO membranes with the interlayer spacing of 0.9 nm as examples, Fig. 10 shows the ACFs of hydrogen bonds in the membranes. The ACF of water in bulk is also presented for comparison. For all the four curves, the c(t) declines with time t increases, indicating a smaller number of water molecules keep hydrogen-bonded. In all the three membranes, the c(t) are higher than that in bulk. This is mainly ascribed to the geometrical confinement as well as the interactions between water and membrane that restrict water diffusion, thereby slowing down the relaxation of hydrogen bonds. Furthermore, the c(t) follows the hierarchy of MXene/GO (40) > MXene/GO(20) > MXene/GO(10), which is in line with the trend of water permeability. This implies that a higher oxidation degree of GO nanosheet in MXene/GO membrane could restrict the relaxation of hydrogen bonds in the membrane and then decline the water permeability.

3.4. Salt rejection

The rejection rate is defined as

$$R = \frac{C_{\text{feed}} - C_{\text{permeate}}}{C_{\text{feed}}} \times 100\%$$

where C_{feed} is the NaCl concentration in the feed side, and C_{permeate} is the one in the permeation side. The salt rejections by MXene/GO membranes are shown in Fig. 11 and listed in Table S2. Generally, the salt rejection decreases with increasing interlayer spacing. When the interlayer spacing of the MXene/GO membrane is 0.6 nm, the salt rejections are all 100%. With increasing oxidation degree of GO nanosheet, the salt rejection accordingly increases. This phenomenon is most evident when the interlayer spacing of the MXene/GO membrane is 1.5 nm. More intriguingly, a 100% rejection is observed in the MXene/GO(40) membrane with the interlayer spacing up to 1.2 nm. As shown in Fig. 1(a), the surface is not that flat when the oxidation degree of the GO surface is up to 40%. Meanwhile, as mentioned in the simulation method, the interlayer spacing is defined as the distance between the carbon in GO and the surface of MXene. Therefore, the functional groups (*e.g.*, the hydroxyl and epoxy groups) occupy the channel in the membrane, which hinders the transport of ions by the steric-hindrance effect. The minimum distances between MXene and GO surface in MXene/GO membranes are analyzed and listed in Table S3. The minimum distances obviously decrease with the increasing oxidation degree of the GO surface, which again illustrates the steric-hindrance effect.

It is worth mentioning that, for MXene/GO(40) membrane with an interlayer spacing of 1.2 nm, the minimum distance between MXene and GO is 0.80 nm (listed in Table S3), which is large enough for the ions to pass through even taking the ionic hydration layer [75] into consideration. However, the ion molecules still can not pass through. To illustrate this, the number densities of ions along z-axis are calculated and plotted in Fig. 12. Two sharp peaks can be found at the entrance and exit of MXene/GO(10) and MXene/GO(20) membranes, *i.e.*, $z = 18.20$ nm and $z = 26.00$ nm,

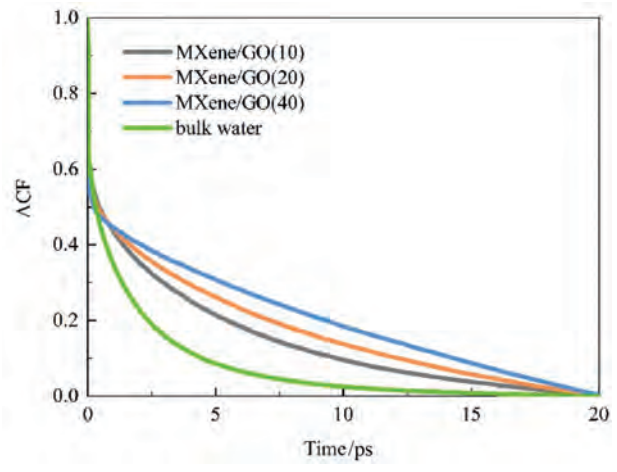

Fig. 10. Autocorrelation function (ACF) of hydrogen bonds in the MXene/GO(10), the MXene/GO(20), and the MXene/GO(40) membranes as well as in bulk water. The interlayer spacings of membranes are 0.9 nm.

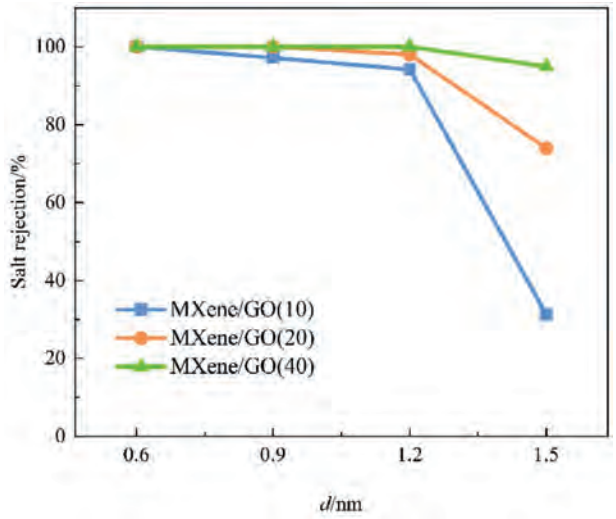

Fig. 11. The salt rejections of MXene/GO membranes. The *x*-axis indicates the interlayer spacing, and the *y*-axis indicates the value of salt rejection.

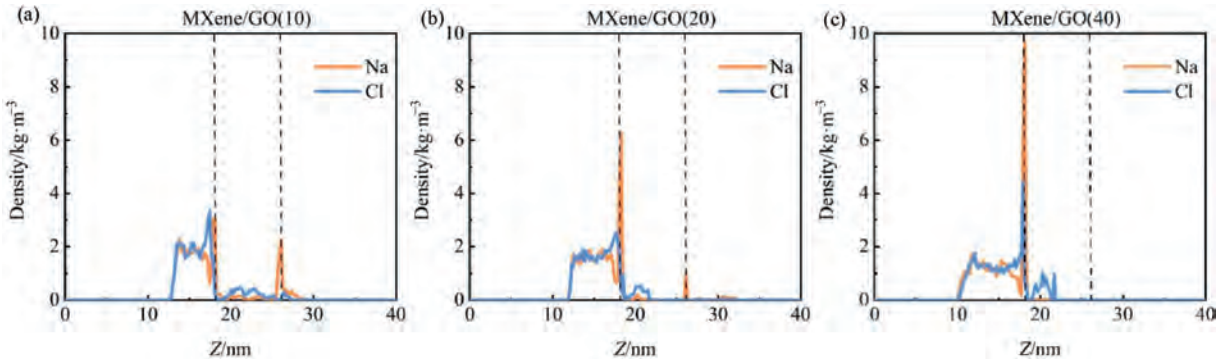

Fig. 12. The number densities of ions along z axis of (a) the MXene/GO(10), (b) the MXene/GO(20), and (c) the MXene/GO(40) membranes with the interlayer spacing of 1.2 nm.

respectively. For the MXene/GO(40) membrane, only one peak can be observed at the entrance because no ion molecule passing through. With the increasing oxidation degree, the density peak becomes stronger. Based on this, we could infer that the accumulation of ions at the interface partially blocks the entrance of the membrane, therefore resulting in a higher rejection, although the interlayer spacing of the membrane is up to 1.2 nm. Overall, the highest water permeability of $37.22 \times 10^{-7}\,L\cdot m^{-1}\cdot h^{-1}\cdot bar^{-1}$ could be observed in the MXene/GO(20) membrane with the interlayer spacing of 0.9 nm, in which the salt rejection remains 100%.

4. Conclusions

In this work, the mechanism of desalination through MXene/GO membranes is systematically investigated using molecular simulation. The effects of interlayer spacing and oxidation degree of GO nanosheets are discussed in detail. Generally, with the increasing interlayer spacing, the water permeability through membranes accordingly increases. The increasing oxidation degree of GO nanosheets would give rise to the reduction of water permeability. Under the same oxidation degree and the interlayer spacing, the water permeability distinctly enhances with the appearance of MXene nanosheets.

The higher water permeability through the MXene/GO membrane is mainly attributed to the ordered orientations as well as the lower transport resistance of water, which are induced by the MXene nanosheet. A higher oxidation of GO nanosheet would result in a stronger interaction with water and a slower relaxation of hydrogen bonds in the membrane.

The salt rejection is mainly determined by the steric-hindrance effect. The highest water permeability of $37.22 \times 10^{-7}\,L\cdot m^{-1}\cdot h^{-1}\cdot bar^{-1}$, along with a salt rejection of 100%, could be observed in the MXene/GO(20) membrane with the interlayer spacing of 0.9 nm. Overall, the results highlight the importance of interfacial effects on water desalination through 2D membranes and provide new insights for the design of new membranes for separation.

CRediT Authorship Contribution Statement

Jie Liu: Writing – original draft, Validation, Investigation, Writing – review & editing, Visualization, Methodology, Conceptualization. Xiaoyan Tan: Visualization, Conceptualization, Writing – original draft, Data curation. Yibo Xu: Methodology, Validation. Zijuan Li: Visualization, Data curation, Validation. Yanan Xue: Writing – review & editing, Data curation, Validation. Faquan Yu: Writing – review & editing, Supervision, Validation, Data curation.

Declaration of Competing Interest

The authors declare that they have no known competing financial interests or personal relationships that could have appeared to influence the work reported in this paper.

Acknowledgements

This work was supported by the National Natural Science Foundation of China (22078251, 21706197); the Open Project of Hubei Key Laboratory of Novel Reactor and Green Chemical Technology (NRG202407); the Ministry-of-Education, Key Laboratory for the Synthesis and Application of Organic Functional Molecules (KLSAOFM2511); the Graduate Innovative Fund of Wuhan Institute of Technology (CX2023024).

Supplementary Material

Supplementary data to this article can be found online at https://doi.org/10.1016/j.cjche.2025.05.033.

References

[1] P. Greve, T. Kahil, J. Mochizuki, T. Schinko, Y. Satoh, P. Burek, G. Fischer, S. Tramberend, R. Burtscher, S. Langan, Y. Wada, Global assessment of water challenges under uncertainty in water scarcity projections, *Nat. Sustain.* 1 (2018) 486–494.
[2] M.M. Mekonnen, A.Y. Hoekstra, Four billion people facing severe water scarcity, *Sci. Adv.* 2 (2) (2016) e1500323.
[3] M. Prajapati, M. Shah, B. Soni, A review of geothermal integrated desalination: a sustainable solution to overcome potential freshwater shortages, *J. Clean. Prod.* 326 (2021) 129412.
[4] K.P. Lee, T.C. Arnot, D. Mattia, A review of reverse osmosis membrane materials for desalination: development to date and future potential, *J. Membr. Sci.* 370 (1–2) (2011) 1–22.
[5] T.S. Chung, S. Zhang, K.Y. Wang, J.C. Su, M.M. Ling, Forward osmosis processes: yesterday, today and tomorrow, *Desalination* 287 (2012) 78–81.
[6] J. Shen, G.P. Liu, Y. Han, W.Q. Jin, Artificial channels for confined mass transport at the sub-nanometre scale, *Nat. Rev. Mater.* 6 (2021) 294–312.
[7] J.D. Yang, Z.K. Li, Z.Y. Wang, S. Yuan, Y. Li, W. Zhao, X.W. Zhang, 2D material based thin-film nanocomposite membranes for water treatment, *Adv. Mater. Technol.* 6 (10) (2021) 2000862.
[8] Y. Kang, Y. Xia, H.T. Wang, X.W. Zhang, 2D laminar membranes for selective water and ion transport, *Adv. Funct. Mater.* 29 (29) (2019) 1902014.
[9] C.N. Yeh, K. Raidongia, J.J. Shao, Q.H. Yang, J.X. Huang, On the origin of the stability of graphene oxide membranes in water, *Nat. Chem.* 7 (2) (2014) 166–170.
[10] S.K. Tiwary, M. Singh, S.V. Chavan, A. Karim, Graphene oxide-based membranes for water desalination and purification, *NPJ 2D Mater. Appl.* 8 (2024) 27.
[11] W.W. Lei, D. Portehault, D. Liu, S. Qin, Y. Chen, Porous boron nitride nanosheets for effective water cleaning, *Nat. Commun.* 4 (2013) 1777.
[12] N. Vafa, A. Hamed Mashhadzadeh, M. Zarghami Dehaghani, B. Firoozabadi, S. Nouranian, C. Spitas, Molecular dynamics simulation of hexagonal boron nitride slit membranes for wastewater treatment, *J. Mol. Liq.* 382 (2023) 121842.

[13] Z.L. Song, Y.L. Niu, J. Yang, L. Chen, J.L. Chen, Comparison of water desalination performance of porous graphene and MoS_2 nanosheets, *RSC Adv.* 12 (42) (2022) 27641–27647.

[14] J.Y. Zhu, W.Q. Meng, Q. Xue, K.S. Zhang, Two dimensional sulfonated molybdenum disulfide (S–MoS_2) thin-film nanocomposite nanofiltration membrane for selective desalination, *J. Membr. Sci.* 676 (2023) 121574.

[15] X.M. Yang, X.N. Yang, Molecular simulation of water permeation and salt rejection for MoS_2 nanoslit membranes, *Desalination* 564 (2023) 116787.

[16] S.W. Liao, Q. Ke, Y.Y. Wei, L.B. Li, Water's motions in *x-y* and *z* directions of 2D nanochannels: entirely different but tightly coupled, *Nano Res.* 16 (5) (2023) 6298–6307.

[17] Y.C. Liu, D.Q. Xie, M.R. Song, L.Z. Jiang, G. Fu, L. Liu, J.Y. Li, Water desalination across multilayer graphitic carbon nitride membrane: insights from non-equilibrium molecular dynamics simulations, *Carbon* 140 (2018) 131–138.

[18] Y.C. Liu, Y.J. Zou, H. Zhu, S. Xie, J.H. Wu, J.L. Li, J.Y. Li, Effect of inhomogeneous structure on the water desalination performance of graphitic carbon nitride nanochannels: a molecular dynamics study, *J. Mol. Liq.* 396 (2024) 123953.

[19] H.E. Karahan, K. Goh, C.J. Zhang, E. Yang, C. Yıldırım, C.Y. Chuah, M.G. Ahunbay, J. Lee, Ş.B. Tantekin-Ersolmaz, Y. Chen, T.H. Bae, MXene materials for designing advanced separation membranes, *Adv. Mater.* 32 (29) (2020) e1906697.

[20] J. Usman, L.T. Yogarathinam, N. Baig, S.I. Abba, R. Chrystie, I.H. Aljundi, MXene-enhanced sulfonated TFN nanofiltration membranes for improved desalination performance, *Desalination* 581 (2024) 117566.

[21] N. Albayati, Z.A. Naser, H.A. Baqi Ahmed, M. Kadhom, P. Olusakin Oladoye, A comprehensive review on the use of $Ti_3C_2T_x$ MXene in membrane-based water treatment, *Sep. Purif. Technol.* 345 (2024) 127448.

[22] M. Berkani, A. Smaali, F. Almomani, Y. Vasseghian, Recent advances in MXene-based nanomaterials for desalination at water interfaces, *Environ. Res.* 203 (2022) 111845.

[23] Y.A.J. Al-Hamadani, B.M. Jun, M. Yoon, N. Taheri-Qazvini, S.A. Snyder, M. Jang, J. Heo, Y. Yoon, Applications of MXene-based membranes in water purification: a review, *Chemosphere* 254 (2020) 126821.

[24] C.E. Ren, K.B. Hatzell, M. Alhabeb, Z. Ling, K.A. Mahmoud, Y. Gogotsi, Charge- and size-selective ion sieving through $Ti_3C_2T_x$ MXene membranes, *J. Phys. Chem. Lett.* 6 (20) (2015) 4026–4031.

[25] L. Ding, Y. Wei, Y. Wang, H. Chen, J. Caro, H. Wang, A two-dimensional lamellar membrane: mxene nanosheet stacks, *Angew. Chem. Int. Ed.* 56 (7) (2017) 1825–1829.

[26] L. Ding, L.B. Li, Y.C. Liu, Y. Wu, Z. Lu, J.J. Deng, Y.Y. Wei, J. Caro, H.H. Wang, Effective ion sieving with $Ti_3C_2T_x$ MXene membranes for production of drinking water from seawater, *Nat. Sustain.* 3 (2020) 296–302.

[27] B.C. Meng, G.Z. Liu, Y.Y. Mao, F. Liang, G.P. Liu, W.Q. Jin, Fabrication of surface-charged MXene membrane and its application for water desalination, *J. Membr. Sci.* 623 (2021) 119076.

[28] H.Y. Luo, N. Xu, Y.N. Li, J.Z. Li, W.L. Ji, P. Nian, Z. Wang, Y.B. Wei, Amino acid-bonded Ti3C2Tx MXene nanofiltration membranes with superior antifouling property for enhanced water purification, *J. Membr. Sci.* 693 (2024) 122384.

[29] R.P. Pandey, K. Rasool, V.E. Madhavan, B. Aïssa, Y. Gogotsi, K.A. Mahmoud, Ultrahigh-flux and fouling-resistant membranes based on layered silver/MXene ($Ti_3C_2T_x$) nanosheets, *J. Mater. Chem. A* 6 (8) (2018) 3522–3533.

[30] X.Y. Ma, A.Q. Wang, J.L. Miao, T.T. Fan, 2D lamellar membrane with MXene hetero-intercalated small sized graphene oxide for harsh environmental wastewater treatment, *Sep. Purif. Technol.* 311 (2023) 123248.

[31] T. Liu, X.Y. Liu, N. Graham, W.Z. Yu, K.N. Sun, Two-dimensional MXene incorporated graphene oxide composite membrane with enhanced water purification performance, *J. Membr. Sci.* 593 (2020) 117431.

[32] G.Y. Zeng, Q.Q. Lin, K. Wei, Y.C. Liu, S.Z. Zheng, Y.Q. Zhan, S.J. He, T. Patra, Y.H. Chiao, High-performing composite membrane based on dopamine-functionalized graphene oxide incorporated two-dimensional MXene nanosheets for water purification, *J. Mater. Sci.* 56 (11) (2021) 6814–6829.

[33] R. Chang, J. Ma, Y.Y. Hou, J.Z. Xu, Graphene oxide intercalated with MXene as composite membranes with improved permeability for wastewater treatment, *ACS Appl. Nano Mater.* 7 (10) (2024) 11749–11756.

[34] X.Y. Ma, T.T. Fan, G. Wang, Z.H. Li, J.H. Lin, Y.Z. Long, High performance GO/MXene/PPS composite filtration membrane for dye wastewater treatment under harsh environmental conditions, *Compos. Commun.* 29 (2022) 101017.

[35] S.C. Wei, Y. Xie, Y.D. Xing, L.C. Wang, H.Q. Ye, X. Xiong, S. Wang, K. Han, Two-dimensional graphene Oxide/MXene composite lamellar membranes for efficient solvent permeation and molecular separation, *J. Membr. Sci.* 582 (2019) 414–422.

[36] S.L. Li, J. Lu, D. Zou, L.L. Cui, B. Chen, F. Wang, J. Qiu, T.X. Yu, Y.Q. Sun, W.H. Jing, Constructing reduced porous graphene oxide for tailoring mass-transfer channels in ultrathin MXene ($Ti_3C_2T_x$) membranes for efficient dye/salt separation, *Chem. Eng. J.* 457 (2023) 141217.

[37] Q. Ke, X.T. Gong, S.W. Liao, C.X. Duan, L.B. Li, Effects of thermostats/barostats on physical properties of liquids by molecular dynamics simulations, *J. Mol. Liq.* 365 (2022) 120116.

[38] L.B. Li, T. Zhang, Y.F. Duan, Y.Y. Wei, C.J. Dong, L. Ding, Z.W. Qiao, H.H. Wang, Selective gas diffusion in two-dimensional MXene lamellar membranes: insights from molecular dynamics simulations, *J. Mater. Chem. A* 6 (25) (2018) 11734–11742.

[39] T. Si, X.Y. Ma, T.R. Wang, S. Tak Chu, J. Fan, Improvement of desalination performance by adjusting the arrangement of lamellar MXene membrane, *Sep. Purif. Technol.* 322 (2023) 124265.

[40] X.Y. Ma, X.H. Zhu, C.X. Huang, J. Fan, Exploring the potential of MXene nanoslit for water desalination through molecular dynamics simulations, *Desalination* 556 (2023) 116560.

[41] X.Y. Ma, X.H. Zhu, C.X. Huang, J. Fan, Revealing the effects of terminal groups of MXene on the water desalination performance, *J. Membr. Sci.* 647 (2022) 120334.

[42] E.Y.M. Ang, T.Y. Ng, J. Yeo, R.M. Lin, Z.S. Liu, K.R. Geethalakshmi, Investigations on different two-dimensional materials as slit membranes for enhanced desalination, *J. Membr. Sci.* 598 (2020) 117653.

[43] K. Meidani, Z.L. Cao, A. Barati Farimani, Titanium carbide MXene for water desalination: a molecular dynamics study, *ACS Appl. Nano Mater.* 4 (6) (2021) 6145–6151.

[44] H.Y. He, J. Klinowski, M. Forster, A. Lerf, A new structural model for graphite oxide, *Chem. Phys. Lett.* 287 (1–2) (1998) 53–56.

[45] A.J.P. Neto, V.V. Chaban, E.E. Fileti, Hydration peculiarities of graphene oxides with multiple oxidation degrees, *Phys. Chem. Chem. Phys.* 19 (48) (2017) 32333–32340.

[46] H.C. Schniepp, J.L. Li, M.J. McAllister, H. Sai, M. Herrera-Alonso, D.H. Adamson, R.K. Prud'homme, R. Car, D.A. Saville, I.A. Aksay, Functionalized single graphene sheets derived from splitting graphite oxide, *J. Phys. Chem. B* 110 (17) (2006) 8535–8539.

[47] A.V. Talyzin, T. Hausmaninger, S.J. You, T. Szabó, The structure of graphene oxide membranes in liquid water, ethanol and water-ethanol mixtures, *Nanoscale* 6 (1) (2014) 272–281.

[48] S. Kim, S. Zhou, Y. Hu, M. Acik, Y.J. Chabal, C. Berger, W. de Heer, A. Bongiorno, E. Riedo, Room-temperature metastability of multilayer graphene oxide films, *Nat. Mater.* 11 (6) (2012) 544–549.

[49] D.X. Yang, A. Velamakanni, G. Bozoklu, S. Park, M. Stoller, R.D. Piner, S. Stankovich, I. Jung, D.A. Field, C.A. Ventrice, R.S. Ruoff, Chemical analysis of graphene oxide films after heat and chemical treatments by X-ray photoelectron and Micro-Raman spectroscopy, *Carbon* 47 (1) (2009) 145–152.

[50] R.Y. Han, P.Y. Wu, High-performance graphene oxide nanofiltration membrane with continuous nanochannels prepared by the *in situ* oxidation of MXene, *J. Mater. Chem. A* 7 (11) (2019) 6475–6481.

[51] F.K. Wang, Z.Y. Wang, S.D. Wang, X.X. Meng, Y. Jin, N.T. Yang, J. Sunarso, S.M. Liu, Mechanically intensified and stabilized MXene membranes *via* the combination of graphene oxide for highly efficient osmotic power production, *J. Membr. Sci.* 647 (2022) 120280.

[52] X. Zhao, Y.A. Che, Y.H. Mo, W.Q. Huang, C. Wang, Fabrication of PEI modified GO/MXene composite membrane and its application in removing metal cations from water, *J. Membr. Sci.* 640 (2021) 119847.

[53] D. Cohen-Tanugi, J.C. Grossman, Water desalination across nanoporous graphene, *Nano Lett.* 12 (7) (2012) 3602–3608.

[54] P. Pazouki, R.A. Stewart, E. Bertone, F. Helfer, N. Ghaffour, Life cycle cost of dilution desalination in off-grid locations: a study of water reuse integrated with seawater desalination technology, *Desalination* 491 (2020) 114584.

[55] K.M. Gupta, J. Liu, J.W. Jiang, A molecular simulation protocol for membrane pervaporation, *J. Membr. Sci.* 572 (2019) 676–682.

[56] W.L. Jorgensen, D.S. Maxwell, J. Tirado-Rives, Development and testing of the OPLS all-atom force field on conformational energetics and properties of organic liquids, *J. Am. Chem. Soc.* 118 (45) (1996) 11225–11236.

[57] W.L. Jorgensen, J. Chandrasekhar, J.D. Madura, R.W. Impey, M.L. Klein, Comparison of simple potential functions for simulating liquid, *water* 79 (2) (1983) 926–935.

[58] Y.C. Liu, Z.W. Cheng, M.R. Song, L.Z. Jiang, G. Fu, L. Liu, J.Y. Li, Molecular dynamics simulation-directed rational design of nanoporous graphitic carbon nitride membranes for water desalination, *J. Membr. Sci.* 620 (2021) 118869.

[59] C. Chen, F. Huang, L.J. Jia, L. Zhang, E.Y. Chen, L.J. Liang, Z. Kong, X.P. Wang, W. Zhang, J.W. Shen, Molecular insights into desalination performance of lamellar graphene membranes: significant of hydrophobicity and interlayer spacing, *J. Mol. Liq.* 333 (2021) 116024.

[60] J.H. Yao, B. Ma, J. Zhang, C. Chen, L. Zhang, X.P. Wang, W. Zhang, L.J. Liang, E. Y. Chen, Understanding the desalination performance of seawater passing through the lamellar BN membranes: effect of interlayer spacing and concentration, *J. Mol. Liq.* 376 (2023) 121356.

[61] M.J. Abraham, T. Murtola, R. Schulz, S. Páll, J.C. Smith, B. Hess, E. Lindahl, GROMACS: high performance molecular simulations through multi-level parallelism from laptops to supercomputers, *SoftwareX* 1 (2015) 19–25.

[62] G. Bussi, D. Donadio, M. Parrinello, Canonical sampling through velocity rescaling, *J. Chem. Phys.* 126 (1) (2007) 014101.

[63] T. Darden, D. York, L. Pedersen, Particle mesh Ewald: an $N\cdot\log(N)$ method for Ewald sums in large systems 98 (12) (1993) 10089–10092.

[64] U. Essmann, L. Perera, M.L. Berkowitz, T. Darden, H. Lee, L.G. Pedersen, A smooth particle mesh Ewald method, *J. Chem. Phys.* 103 (19) (1995) 8577–8593.

[65] W. Humphrey, A. Dalke, K. Schulten, VMD: visual molecular dynamics, *J. Mol. Graph.* 14 (1) (1996) 33–38.

[66] K.M. Kang, D.W. Kim, C.E. Ren, K.M. Cho, S.J. Kim, J.H. Choi, Y.T. Nam, Y. Gogotsi, H.T. Jung, Selective molecular separation on $Ti_3C_2T_x$-graphene oxide membranes during pressure-driven filtration: comparison with graphene oxide and MXenes, *ACS Appl. Mater. Interfaces* 9 (51) (2017) 44687–44694.

[67] S.W. Liu, S. Keten, R.M. Lueptow, Effect of molecular dynamics water models on flux, diffusivity, and ion dynamics for polyamide membrane simulations, *J. Membr. Sci.* 678 (2023) 121630.
[68] J.H. Wang, Self-diffusion coefficients of water, *J. Phys. Chem.* 69 (12) (1965) 4412.
[69] K.T. Gillen, D.C. Douglass, M.J.R. Hoch, Self-diffusion in liquid water to−31°C, *J. Chem. Phys.* 57 (12) (1972) 5117–5119.
[70] R. Mills, Self-diffusion in normal and heavy water in the range 1-45.deg, *J. Phys. Chem.* 77 (5) (1973) 685–688.
[71] H.W. Dai, Z.J. Xu, X.N. Yang, Water permeation and ion rejection in layer-by-layer stacked graphene oxide nanochannels: a molecular dynamics simulation, *J. Phys. Chem. C* 120 (39) (2016) 22585–22596.
[72] G. Algara-Siller, O. Lehtinen, F.C. Wang, R.R. Nair, U. Kaiser, H.A. Wu, A.K. Geim, I.V. Grigorieva, Square ice in graphene nanocapillaries, *Nature* 519 (7544) (2015) 443–445.
[73] A.K. Giri, F. Teixeira, M.N.D.S. Cordeiro, Salt separation from water using graphene oxide nanochannels: a molecular dynamics simulation study, *Desalination* 460 (2019) 1–14.
[74] Q. Tan, Y. Fan, Z.L. Song, J.L. Chen, L. Chen, Effects of interlayer spacing and oxidation degree of graphene oxide nanosheets on water permeation: a molecular dynamics study, *J. Mol. Model.* 28 (3) (2022) 57.
[75] J. Zhou, X.H. Lu, Y.R. Wang, J. Shi, Molecular dynamics study on ionic hydration, *Fluid Phase Equilib.* 194 (2002) 257–270.